CHAPTER 3

Spin freezing and Field induced transition in $(Tb_{1-x}Eu_x)_2Ti_2O_7$: A Magnetic Property study

3.1 Introduction:

Geometrically frustrated pyrochlore systems $A_2B_2O_6O'$ where A is a rare earth ion and B is transition metal ion [4], have attracted great attention both experimentally and theoretically since past decades owing to their different low temperature states [10, 150-152]. In frustrated pyrochlore system, a balance between exchange interactions, dipolar interactions, single ion anisotropy and strong crystal field effects lead to a formation of exotic degenerate ground states [12, 153, 154]. These ground states include spin liquid [39, 155], spin glass [156-158], spin ice [159-160] and order by disorder systems [31, 161-162]. In cubic pyrochlore oxide $R_2Ti_2O_7$ (space group Fd-3m), the Ti^{4+} ions are non-magnetic and the rare earth ion R^{3+} which resides on a lattice of corner sharing tetrahedron has a key role to determine the magnetic properties. In this geometry, each R^{3+} ion is surrounded by 8 oxygen atoms showing a distorted trigonal cube of D_{3d} symmetry which leads to frustration [163]. A difference is created between the R^{3+} ionic magnetic susceptibilities along D_{3d} axis and its perpendicular direction due to strong crystal field interaction with the D_{3d} symmetry which in turn helps in developing single ion anisotropy [65]. The pyrochlore structure with specific antiferromagnetic exchange interaction shows no transition to long range magnetic ordering at finite temperature although its classical Heisenberg magnetic moment interacts with nearest neighbour [5-8]. It has been suggested that, such magnetic systems, i.e., *S=1/2* Heisenberg antiferromagnetic pyrochlores are fully quantum disordered. They possess a spin liquid state which has strong and non–trivial short range spin correlations [9]. Interestingly, some insulating magnetic systems are known to show either long range ordering as in FeF_3 [164], $Gd_2Ti_2O_7$ [165-166], $ZnFe_2O_4$ [167] and $ZnCr_2O_4$ [168] or spin glass phase as in $Y_2Mo_2O_7$ [169-171], $Tb_2Mo_2O_7$ [172], $Y_2Mn_2O_7$ [173], $CsNiCrF_6$ [174] pyrochlore etc.

In the present investigation, we have studied $(Tb_{1-x}Eu_x)_2Ti_2O_7$ (TETO). One of our parent compound spin liquid $Tb_2Ti_2O_7$ (TTO) has ideal ordered structure as it is free from A/B disorder or oxygen non-stoichiometry [175]. Deviation in Tb/Ti ratio is known to influence the spin lattice coupling below 1 K [176]. Negative Curie-Weiss temperature (θ_{CW} = -14.75 K) of TTO confirms the effective antiferromagnetic interaction between the spins. Therefore, magnetic frustration should not develop due to <111> anisotropy and one expects a long range magnetic ground state. However, no long range magnetic ordering has been evidenced down to 50 mK [37, 177-178]. From different measurements such as elastic and inelastic neutron scattering (INS), muon spin relaxation (μSR), it has been observed that AFM short range order develops around 50 K in this pyrochlore, but the system remains in paramagnetic state down to 0.05 K [177]. However, a partial spin freezing has been observed for TTO below 350 mK from AC susceptibility measurement [179]. Similar result has been revealed from neutron spin echo measurement where a partial spin freezing (~20% frozen spins) of the Tb spins below 0.3 K was observed. This was explained on the basis of the presence of small number of defects in the system. The partially frozen spins are situated at such defect lattice sites [15]. Recently, a strong elastic scattering below 275 mK has been reported for $Tb_2Ti_2O_7$ from high resolution neutron scattering. This elastic scattering was developed due to presence of some spin glass type behaviour below 275 mK [180]. Further from a recent report, it has been proposed that $Tb_2Ti_2O_7$ crystal possesses two phases at low temperature and low magnetic field applied along (111) direction [181]. In the field dependent AC susceptibility measurement of TTO, two weak magnetization plateaus were found at temperatures 16 mK and 40 mK which correspond to quantum spin ice and quantum Kagome ice respectively [181].

Another parent compound $Eu_2Ti_2O_7$ (ETO) is also antiferromagnetic in nature (θ_{CW} = -1.35 K) [67]. From earlier magnetic and specific heat studies at low temperature it has been observed that $Eu_2Ti_2O_7$ has temperature dependent anomalous correlation effect in χ^{-1} [66]. It has been shown that this effect is due to the super-exchange interactions between Eu^{3+} ions at intrinsic and defect states [66]. Interestingly, in a recent study, a thermally activated sharp spin freezing around 32 K has been observed in ETO from AC susceptibility measurement [67]. From Cole-Cole plot and Casimir–du Pre relation, it has also been confirmed that this high temperature spin freezing is a single ion relaxation mechanism [67].

In this chapter, we have investigated the structural, magnetic properties and Raman effect of TETO series over the composition range between $Tb_2Ti_2O_7$ and $Eu_2Ti_2O_7$. DC magnetic study indicates a decrease in total magnetic moment on increasing the Eu content. AC magnetic study reveals the appearance of a new field induced peak at lower temperature with the application of a field of 10 kOe. Furthermore, $Tb_2Ti_2O_7$ shows a glass like transition around 33 K at zero magnetic field. Such high temperature partial spin freezing has not been reported yet.

3.2 Experiment:

Polycrystalline samples of $(Tb_{1-x}Eu_x)_2Ti_2O_7$ with (x= 0, 0.25, 0.50, 0.90, 0.95, 1.0) were synthesized using the solid state reaction method. High purity (99.999%) powder of Tb_4O_7, Eu_2O_3 and TiO_2 were taken in an appropriate stoichiometric ratio and ground for half an hour and then heated at 1000 ^oC in air for 24 hours. This calcination process was repeated several times. The resulting powder were pressed into pellets and sintered at 1400 ^oC for 48 hours. The prepared samples were characterized by X- ray powder diffraction (XRD) method at

room temperature by using Rigaku Miniflex II X-ray diffractometer using Cu Kα radiation. All the DC and AC magnetic measurements were carried out using a Quantum Design magnetic property measurement system (MPMS) super conducting quantum interference device (SQUID) magnetometer. Raman spectra were recorded using a Renishaw Micro Raman Spectrometer using a solid state Laser of wavelength 532 nm.

3.3 Results and Discussions:

3.3.1 Stability Study:

Formation and stability of $R_2Ti_2O_7$ pyrochlores mainly depend on the ionic radius of R^{3+} and Ti^{4+} cations. If the ionic radius ratio (IRR) $r(R^{3+})/r(Ti^{4+})$ lies between 1.46 - 1.78, it forms a pyrochlore structure. The system becomes a defect fluorite if the ratio is less than 1.46 and a larger value of the ratio (> 1.78) produces a pervoskite layered structure [182]. We have calculated the IRR of TETO samples using this equation [183]:

$$\frac{r(R^{3+})}{r(Ti^{4+})} = \frac{(1-x)r(Tb^{3+}) + xr(Eu^{3+})}{r(Ti^{4+})} \quad (3.1)$$

To calculate IRR, we have taken the Shannon ionic radius of Tb^{3+}, Eu^{3+}, Ti^{4+} (according to their Coordination number) ions which are 1.04 Å , 1.066 Å , 0.605 Å respectively.

The calculated values are arranged in Table 3.1. It is clear from table 3.1 that the IRR for all the samples lies in the range 1.46 - 1.78. Hence, all TETO samples are shaped into pyrochlore structure. However, the IRR is increasing with increase of Eu^{3+} content and as a consequence disorder in their structure is also increasing with Eu concentration.

Sample	$Tb_2Ti_2O_7$	$Tb_{1.5}Eu_{0.5}Ti_2O_7$	$Tb_{1.0}Eu_{1.0}Ti_2O_7$	$Tb_{0.2}Eu_{1.8}Ti_2O_7$	$Tb_{0.1}Eu_{1.9}Ti_2O_7$	$Eu_2Ti_2O_7$
$r(R^{3+})/r(Ti^{4+})$	1.72	1.73	1.74	1.75	1.76	1.762

Table 3.1: The ionic radius ratio of TETO series compounds.

3.3.2 Structural Study:

The XRD patterns of TETO samples are shown in Figure 3.1. All the samples were formed in single phase with no impurity. The enlarged view of the diffraction peak (222) of TETO series is presented in the inset (i) of Figure 3.1. As the doping concentration is increased, the diffraction peak (222) is found to be shifted towards lower angles. The shifting of the peak to the lower angle side can be attributed to the fact that the ionic radius of Eu^{3+} ion is larger than that of the Tb^{3+} ion resulting in increase in the lattice parameter. Thus, from this feature, it is clear that the Eu^{3+} ions successfully replace the Tb^{3+} ions in all the samples. We have also extracted the values of lattice constant (listed in table 3.2) of all the samples from Rietveld refinement using FULLPROF program [184].

Parameters	x = 0	x = 0.25	x = 0.50	x = 0.90	x = 0.95	x = 1.0
Lattice Constant (Å)	10.155	10.163	10.175	10.191	10.199	10.209
Cell Volume ($Å^3$)	1047.136	1049.689	1053.487	1058.464	1061.083	1064.057

Table 3.2: Lattice parameters obtained from rietveld refinement of all TETO compositions with Space Group Fd-3m.

The refined diagram of $Tb_{1.0}Eu_{1.0}Ti_2O_7$ is shown in inset (ii) of Figure 3.1. From the table it is found that the lattice constants of all the samples increase quasi-linearly with increase in Eu^{3+} content.

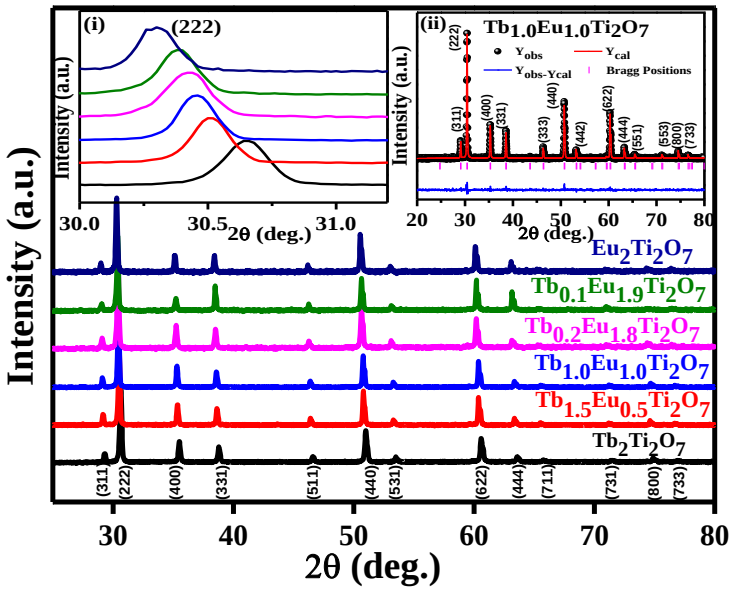

Figure 3.1: Powder x-ray diffraction pattern for the $(Tb_{1-x}Eu_x)_2Ti_2O_7$ samples. Inset (i): Diffraction peak (222) of $(Tb_{1-x}Eu_x)_2Ti_2O_7$ samples. Inset (ii): Rietveld refinement for the $Tb_{1.0}Eu_{1.0}Ti_2O_7$ sample.

3.3.3 Raman Study:

Figure 3.2a shows the Raman spectra of TETO series at 300 K in which the bands were assigned according to the reported data [185-189]. Phonon band near 512 cm^{-1} is assigned to A_{1g} mode. From the temperature dependent Raman study of $Tb_2Ti_2O_7$, it was previously found that there were two peaks at 291 cm^{-1} and 331 cm^{-1} at 4.2 K corresponding to F_{2g} and E_g bands respectively [185-189]. The E_g band weakens at room temperature [185-189].

Therefore, the most intense peak in the present investigation at 297 cm^{-1} can be assigned to a combination of two phonon modes [F_{2g}+E_g]. The fourth mode near 451 cm^{-1} which has a weak signal, is assigned to F_{2g} mode. Among the rest two F_{2g} phonon modes, the one at 209 cm^{-1} is visible in the present case, but another one near 557 cm^{-1} is missing. The peak at 682 cm^{-1} is assigned to the combination mode instead of forbidden IR mode [46].

The variation of phonon modes with the increasing concentration of Eu^{3+} for all the samples is shown in Figure 3.2b. For the combined F_{2g}+E_g (297 cm^{-1}) and F_{2g} (209 cm^{-1}) mode, blue shift i.e. hardening of modes is observed, whereas for F_{2g} (451 cm^{-1}) and A_{1g} (512 cm^{-1}) modes, red shift i.e. softening of mode is found. Generally, the locations of Raman active bands depend on the bond strength, bond length and ionic masses. In present investigation, the lattice parameters of compounds are increasing continuously on increasing the concentration of Eu. Due to these factors, the phonon modes should shift to lower frequencies for TETO series as shown in Figure 3.2b for A_{1g} (512 cm^{-1}) mode and F_{2g} (451 cm^{-1}) modes. But, for F_{2g}+E_g (297 cm^{-1}) and another F_{2g} (209 cm^{-1}) mode, a hardening behavior of modes has been observed. This hardening behaviour of phonon modes arises due to strong phonon – phonon anharmonic interaction in the system [190-191]. The gradual shift in all the phonon modes observed in Raman analysis again confirms the successful substitution of Tb ions by Eu ions.

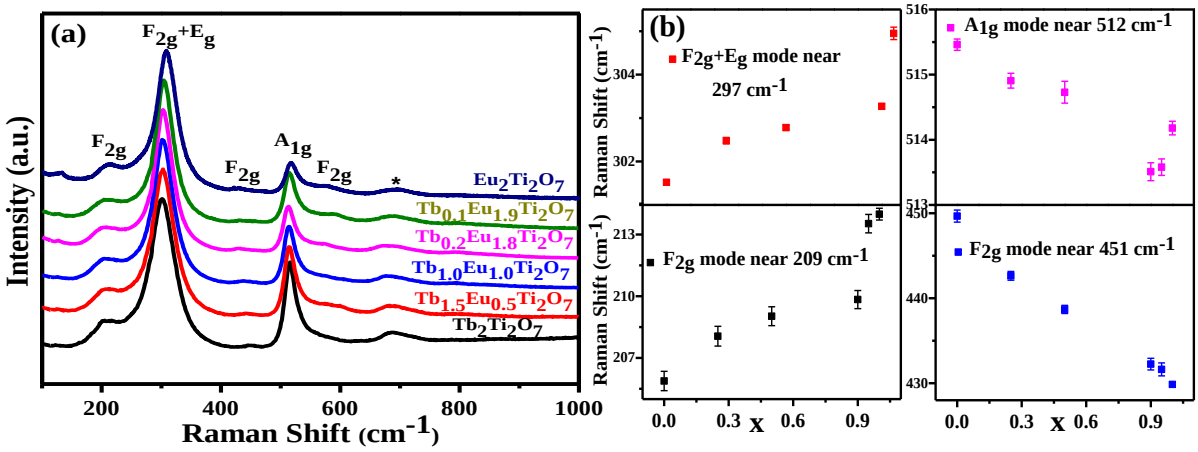

Figure 3.2(a): Raman Spectra of the $(Tb_{1-x}Eu_x)_2Ti_2O_7$ samples at 300 K. **(b)**: Variation of all four active phonon modes as a function of x in $(Tb_{1-x}Eu_x)_2Ti_2O_7$ samples .

3.3.4 DC Magnetic Study:

In order to investigate the magnetic property of the TETO, we have measured the temperature and magnetic field dependent DC magnetization. Figure 3.3a shows temperature dependent magnetization of all the samples at zero field cooled (ZFC) condition which reveals a paramagnetic behaviour. From the *M-T* curves, it can be observed that spin liquid compound TTO possesses highest magnetic moment among all the samples due to presence of Tb^{3+} ion. When Tb^{3+} ion is substituted by the Eu^{3+} ion, the magnetic moment decreases and becomes minimum for $Eu_2Ti_2O_7$ as Eu ion is non-magnetic in its ground state. An interesting feature is observed in inverse DC susceptibility (χ^{-1}) vs. temperature curve (shown in Figure 3.3c). The χ^{-1} for the first three samples (x = 0, 0.25, 0.50) show linear behaviour with temperature due to the presence of strong crystal field interactions. On the other hand, samples with larger Eu^{3+} content (x = 0.90, 0.95, 1.0), show sharp drop down with decrease in temperature due to weak crystal field interactions at low temperature (below 5 K). This

indicates the presence of other magnetic interactions *viz.* exchange, dipolar interactions etc. [192]. Due to this interesting observation, we have analyzed the χ^{-1} data in three parts.

(A) We have fitted the χ^{-1} data for x = 0, 0.25, 0.50 samples with Curie-Weiss (CW) law;

$$\chi^{-1} = \frac{T}{C} - \frac{\theta_{CW}}{C} \tag{3.2}$$

Where, θ_{CW} is Curie - Weiss temperature and *C* is Curie constant. From inset of Figure 3.3d, it can be seen that inverse DC susceptibility data is fitted well in temperature range 25-300 K. The theoretical effective magnetic moment of all the samples is calculated using the relation;

$$\mu^2_{eff} = x\mu^2_{Tb} + y\mu^2_{Eu} \tag{3.3}$$

Where, *x* and *y* are number of Tb and Eu atoms per f.u. respectively. μ_{Tb} and μ_{Eu} are the effective magnetic moment of Tb and Eu ions respectively. From Curie - Weiss fit, the effective magnetic moment is calculated using $C = \frac{N\mu^2_{eff}}{3k}$, where *N* is Avogadro's number and *k* is Boltzmann constant. The values obtained from the Curie - Weiss fit are listed in Table 3.3. For $Tb_2Ti_2O_7$, the θ_{CW} is -14.75 K and effective magnetic moment is 9.29 μ_B/Tb^{3+} ion which are consistent with earlier report [37]. The remaining two samples (x = 0.25, 0.50) show higher negative θ_{CW}, corresponds to stronger antiferromagnetic interactions.

Sample	θ_{CW} **(K)**	**Theoretical** (μ_{eff})	**Calculated** (μ_{eff})
$\mathbf{Tb_2Ti_2O_7}$	-14.75	9.5	9.29
$\mathbf{Tb_{1.5}Eu_{0.5}Ti_2O_7}$	-19.8	8.41	8.66
$\mathbf{Tb_{1.0}Eu_{1.0}Ti_2O_7}$	-24.12	7.12	7.313

Table 3.3: Curie–Weiss temperature, theoretical and calculated magnetic moment of (x = 0.00, 0.25, 0.50) samples obtained from Curie–Weiss fit (25-300 K).

(B) We have also fitted the χ^{-1} with Curie-Weiss law for samples for x = 0.90 and x = 0.95 (not shown) in higher temperature range (150 – 300 K) where crystal field interactions are dominant. We have calculated the effective magnetic moment for these three samples whose values are listed in table 3.4.

Sample	Theoretical (μ_{eff})	Calculated (μ_{eff})
$Tb_{0.2}Eu_{1.8}Ti_2O_7$	4.47	5.25
$Tb_{0.1}Eu_{1.9}Ti_2O_7$	4.18	4.704

Table 3.4: Theoretical and calculated magnetic moment of (x = 0.90, 0.95) samples obtained from Curie–Weiss (150-300 K) fit.

(C) To find out the contribution of nearest neighbour exchange interaction energy (J_{nn}) and dipolar interaction energy (D_{nn}), we have fitted the data of Eu rich samples (which show unexpected behaviour at low temperature) with the high temperature series expansion of the susceptibility i.e.,

$$\chi = C\left[\left(\frac{1}{T}\right) + \left(\frac{\theta_{CW}}{T^2}\right)\right] \quad (3.4)$$

We have plotted χT vs. $1/T$ as shown in Figure 3.3d and from the plot, the θ_{CW} values, effective magnetic moment (μ_{eff}), J_{nn} and D_{nn} have been extracted. Here we have considered only classical interactions so the classical exchange interaction energy (J^{cl}) can be calculated using the relation $J^{cl} = S(S+1)J_{nn}$ and $J_{nn} = 3\theta_{CW}/zS(S+1)$ [here $z = 6$ is the co-ordination

number]. The dipolar interaction energy is determined using the relation $D_{nn} = \frac{\mu_0 \mu_{eff}^2}{4\pi\, r_{nn}^3}$ where, r_{nn} is the distance between a R^{3+} ion at (*0, 0, 0*) and its nearest neighbour at (*a/4, a/4, 0*), *a* is the lattice constant of the unit cell of the compound [66]. Using these relations, the calculated parameters are displayed in table 3.5.

Sample	θ_{CW} **(K)**	J^{cl} **(K)**	D_{nn} **(K)**	**Calculated** (μ_{eff})
$Tb_{0.2}Eu_{1.8}Ti_2O_7$	-0.811	-0.406	0.1179	2.98
$Tb_{0.1}Eu_{1.9}Ti_2O_7$	-0.85	-0.4275	0.04058	1.75
$Eu_2Ti_2O_7$	-1.35	-0.6742	0.00609	0.679

Table 3.5: Curie–Weiss temperature, classical exchange energy, dipolar interaction energy and calculated magnetic moment of (x = 0.90, 0.95, 1.0) samples obtained from the fitting of the High Temperature Series Expansion [2-5 K].

It is significant to observe that on increasing the concentration of Eu ions, the classical exchange interaction energy is dominant over dipolar interaction energy which is the reason for enhancement of AFM nature and decrease in effective magnetic moment. The effective theoretical and calculated (from Curie-Weiss fit) magnetic moment of all the compounds at room temperature are comparable as presented in the inset of Figure 3.3b and table 3.3, 3.4.

The variations of magnetization of all compounds with applied magnetic field (*M-H* curves) at 2 K are shown in Figure 3.3b. *M-H* curves of TETO show unsaturated linear nature i.e. magnetic moment does not saturate up to 20 kOe applied magnetic field. This confirms the antiferromagnetic interaction and also supports the decrease of magnetic moment with the increase of Eu content due to the enhancement of AFM exchange interactions.

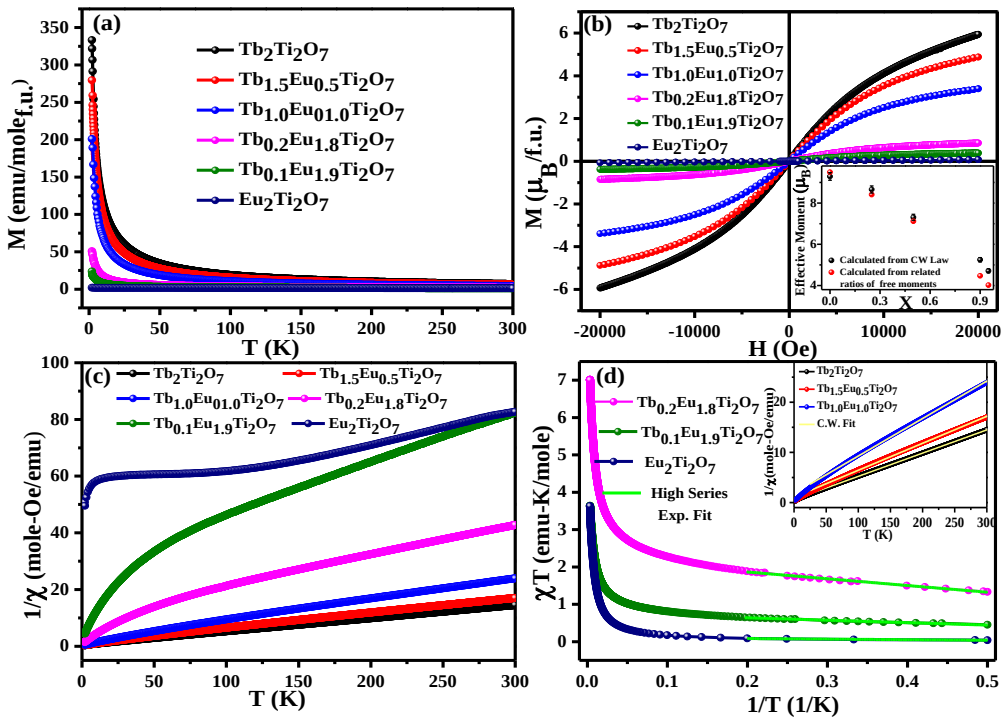

Figure 3.3(a): The temperature dependent magnetization (ZFC) of the $(Tb_{1-x}Eu_x)_2Ti_2O_7$ samples. **(b)**: M(H) at 2 K for all TETO samples. Inset: Variation of effective magnetic moments with Eu content (x) derived from Curie–Weiss Law at high temperature for TETO sample. **(c):** The inverse DC susceptibility of $(Tb_{1-x}Eu_x)_2Ti_2O_7$ samples. **(d):** High Temperature Series Expansion fit for $(Tb_{1-x}Eu_x)_2Ti_2O_7$ (x = 0.90, 0.95, 1.0) samples. Inset: Curie–Weiss fit for $(Tb_{1-x}Eu_x)_2Ti_2O_7$ (x = 0, 0.25, 0.50) samples.

3.3.5 AC magnetic Study:

In order to investigate the spin relaxation mechanism, we have performed AC susceptibility measurement for all the samples. In $Tb_2Ti_2O_7$ at zero applied field, real part of AC susceptibility $\chi'(T)$ (shown in Figure 3.4a) shows canonical paramagnetic behaviour without any anomaly as reported earlier [192]. The imaginary part of the AC susceptibility $\chi''(T)$ in the temperature range 30 - 40 K (inset (i) of Figure 3.4a) shows a relaxation peak around T_f = 33 K which shifts towards higher temperature while increasing frequency.

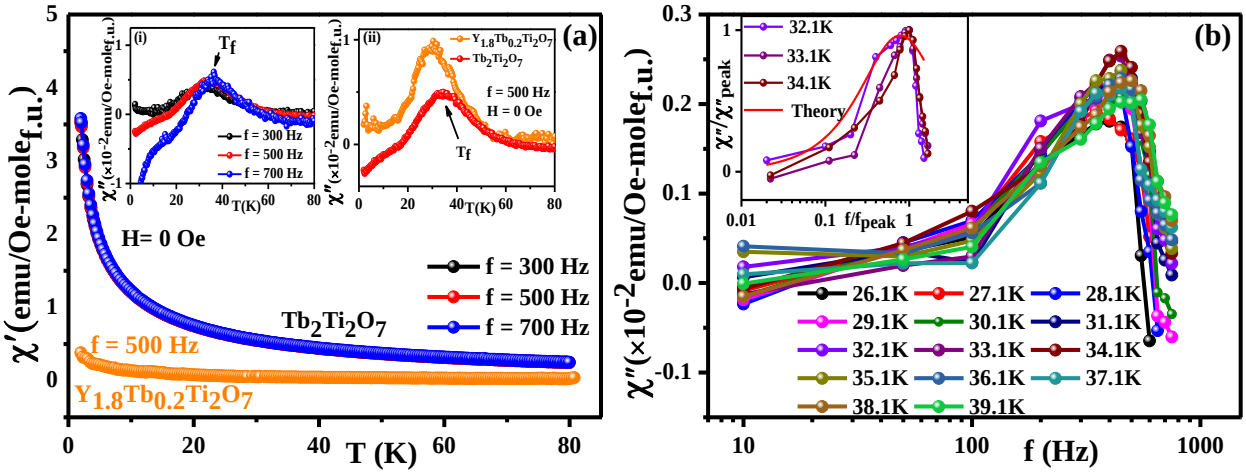

Figure 3.4(a): $\chi'(T)$ of $Tb_2Ti_2O_7$ (f = 300, 500, 700 Hz) and YTTO (f = 500 Hz) at zero applied DC field. Inset (i): $\chi''(T)$ of $Tb_2Ti_2O_7$. Inset (ii): $\chi''(T)$ of TTO and YTTO compounds at H = 0 Oe (500 Hz). **(b):** $\chi''(f)$ at different temperatures for $Tb_2Ti_2O_7$. Inset: Normalized χ'' as a function of f/f_{peak} and fitted theoretically (red) by Casimir du pre relations at and near the transition temperature for $Tb_2Ti_2O_7$.

This transition is thermally activated as it follows the Arrhenius law $f = f_0 \exp(E_a/k_bT)$, where E_a is the activation energy for spin fluctuation, f_0 is a measure of the microscopic limiting frequency in the system and k_B is the Boltzmann constant. The Arrhenius plot of TTO is shown in inset of Figure 3.7a. To investigate the nature of spin freezing, we have calculated the Mydosh parameter, $p = \frac{\Delta T_f}{T_f \Delta(log f)}$. In this expression, p is the parameter which should be less than 0.01 for spin glass transition and T_f is the freezing temperature at frequency f [160]. In the case of TTO, p value is found to be 0.36, suggesting a non spin glass type transition. Moreover, the magnetic field of 10 kOe does not affect the T_f , supporting non spin glass nature of the system [160]. Similar spin freezing transition has also been reported in ETO at 35 K [67]. Although, a partial spin freezing has been reported for TTO at very low temperature (below 350 mK) by different techniques [10, 179, 180]. It is also observed that the energy gap between the first excited and the ground state of the Tb^{3+} CF levels are gradually decreased from 0.37 THz to 0.25 THz when the temperature is

decreased from 30 K to 100 mK [39, 178]. Hence, the observation of the week spin freezing below 33 K in the present report may be associated to the gradual decrease in the CF levels which is also expected as the observed spin freezing is single ion in nature. However, the present higher temperature partial spin freezing is completely new and thus, it is very interesting. It can be useful to improve the understanding of the spin dynamics of this spin liquid compound. Considering the relaxation mechanism to be of spin freezing, further analysis has been carried out. For particular frequency distribution analysis, we have varied the frequency from 10 to 1000 Hz .The variation of χ'' as a function of the frequency f at different temperatures is shown in Figure 3.4b. In this graph, a relatively sharp peak for spin freezing transition at T_f = 33 K has been observed with a maximum value of $\chi''(f)$ at 500 Hz frequency. This spin freezing transition of $Tb_2Ti_2O_7$ is indicating a single ion relaxation process, as frequency dependence of χ'' normalized to its maximum value satisfies the Casimir - du Pre relation, $[\chi''(f)=f\tau\{(\chi_T - \chi_S)/(1+f^2\tau^2)\}]$, where χ_T is isothermal susceptibility in the limit of low frequency and χ_S is the adiabatic susceptibility in the limit of high frequency [193] (shown in inset of Figure 3.4b). However, the expected semicircle in the Cole -Cole (Argand) plot of *"χ' vs χ''",* was not found in TTO (not shown here) [122]. This behaviour may arise due to the frequency independence of $\chi'(T)$ at spin freezing temperature. Thus, it can be concluded that this glassy behaviour in $Tb_2Ti_2O_7$ is not a spin glass, but a partial spin freezing [39]. Furthermore, this featureless behavior of $\chi'(T)$ around freezing temperature could be due to a faster spin relaxation in $\chi'(T)$ of TTO. Moreover, non magnetic dilution of Y^{3+} in TTO system i.e. [$Y_{1.8}Tb_{0.2}Ti_2O_7$ (YTTO)] also shows similar single ion spin freezing. From Figure 3.4a and inset (ii) of Figure 3.4a, the $\chi'(T)$ and $\chi''(T)$ of both YTTO

and pure TTO samples indicate that non magnetic dilution enhances the spin freezing instead of suppressing it.

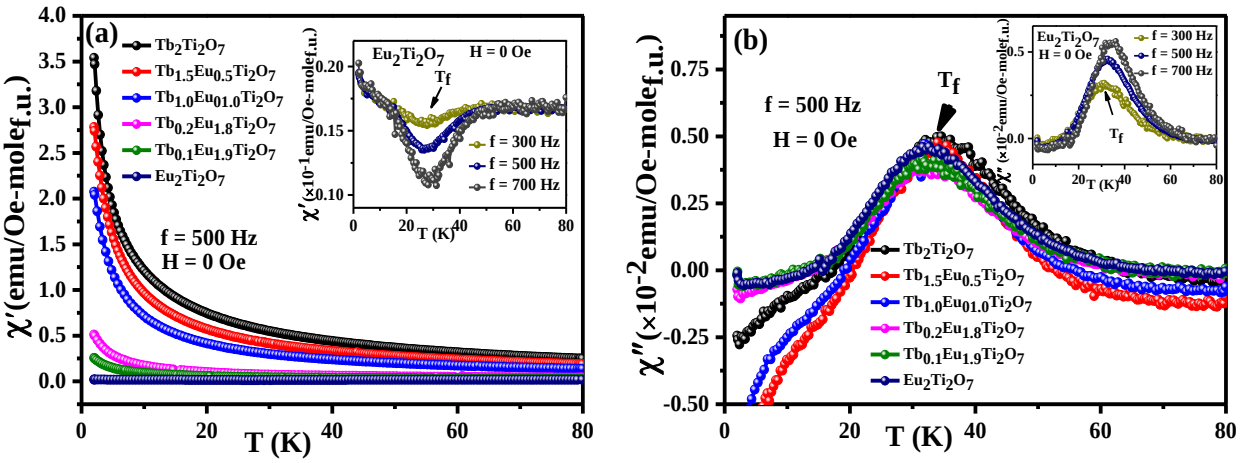

Figure 3.5(a): $\chi'(T)$ of all TETO compounds measured at H = 0 Oe (f = 500 Hz). Inset: χ'(T) of ETO at H = 0 Oe. **(b):** $\chi''(T)$ of all TETO compounds measured at H = 0 Oe (f = 500 Hz). Inset: $\chi''(T)$ of ETO at H = 0 Oe.

It is quite interesting to see the role of Eu^{3+} ions on the spin relaxation mechanism or spin freezing of TTO compound. The temperature dependence of χ' and χ'' of all the systems at zero magnetic field (H = 0 Oe) and at 500 Hz frequency are shown in Figure 3.5. $\chi'(T)$ shows a canonical paramagnetic behaviour of all the compositions except ETO (Figure 3.5a). It is also seen that $\chi'(T)$ of TETO decreases continuously with increasing Eu^{3+} content. ETO compound shows appearance of a clear dip around 35 K in $\chi'(T)$ [inset of Figure 3.5a] and in $\chi''(T)$ corresponding to the dip in $\chi'(T)$ a clear spin freezing transition at a temperature T_f has been observed [inset of Figure 3.5b]. In Figure 3.5b, the $\chi''(T)$ of all the samples show a single ion spin freezing below 35 K. TTO shows a spin freezing at 33 K and ETO shows a spin freezing near 32 K. As, these transitions are close to each other, they are hardly separable in TETO series. All the samples show thermally activated mechanism. Therefore, we have performed the Arrhenius fit of TETO compounds as shown in Figure 3.7a. From the

fit, we have extracted the value of E_a (thermal energy barrier) and f_0 (characteristic frequency). The values of E_a are 198.65 K, 182.946 K, 184.94 K, 186.30 K for x= 0.25, 0.50, 0.90, 0.95 respectively and values of f_0 for all the compositions are around 10^5 Hz. This relatively high value of characteristic relaxation time ($\tau_0 = 1/ f_0$) suggests towards slow spin relaxation occurring near the freezing temperature. The change in E_a values might be due to the small alteration in the crystal field levels as the lattice constant is increased with increase in Eu concentration.

To observe the effect of magnetic field on the AC susceptibility, a field of 10 kOe was applied. Figure 3.6 shows the AC susceptibility data of some of the TETO samples under 10 kOe magnetic field. In upper panel of Figure 3.6a, a field induced transition peak appears at low temperature in χ'(T) of TTO sample. This field induced peak is well established for TTO at stronger magnetic field (>40 kOe) and for higher frequencies (≥1 kHz) [45, 194]. But in the present investigation, this field induced transition peak is not evidenced in $\chi''(T)$ as a sudden jump arises at lower temperature as shown in lower panel of Figure 3.6a. This unusual feature in $\chi''(T)$ part might be due to the fact that Tb^{3+} spins get relaxed faster in the reported frequency range (<1 kHz) below 10 K. As a matter of fact, the peak is not well reproduced due to our limited frequency range. The emergence of this field induced transition in TTO is due to single moment saturation process as the susceptibility part goes to zero for both high and low temperatures in presence of 10 kOe magnetic field [45].

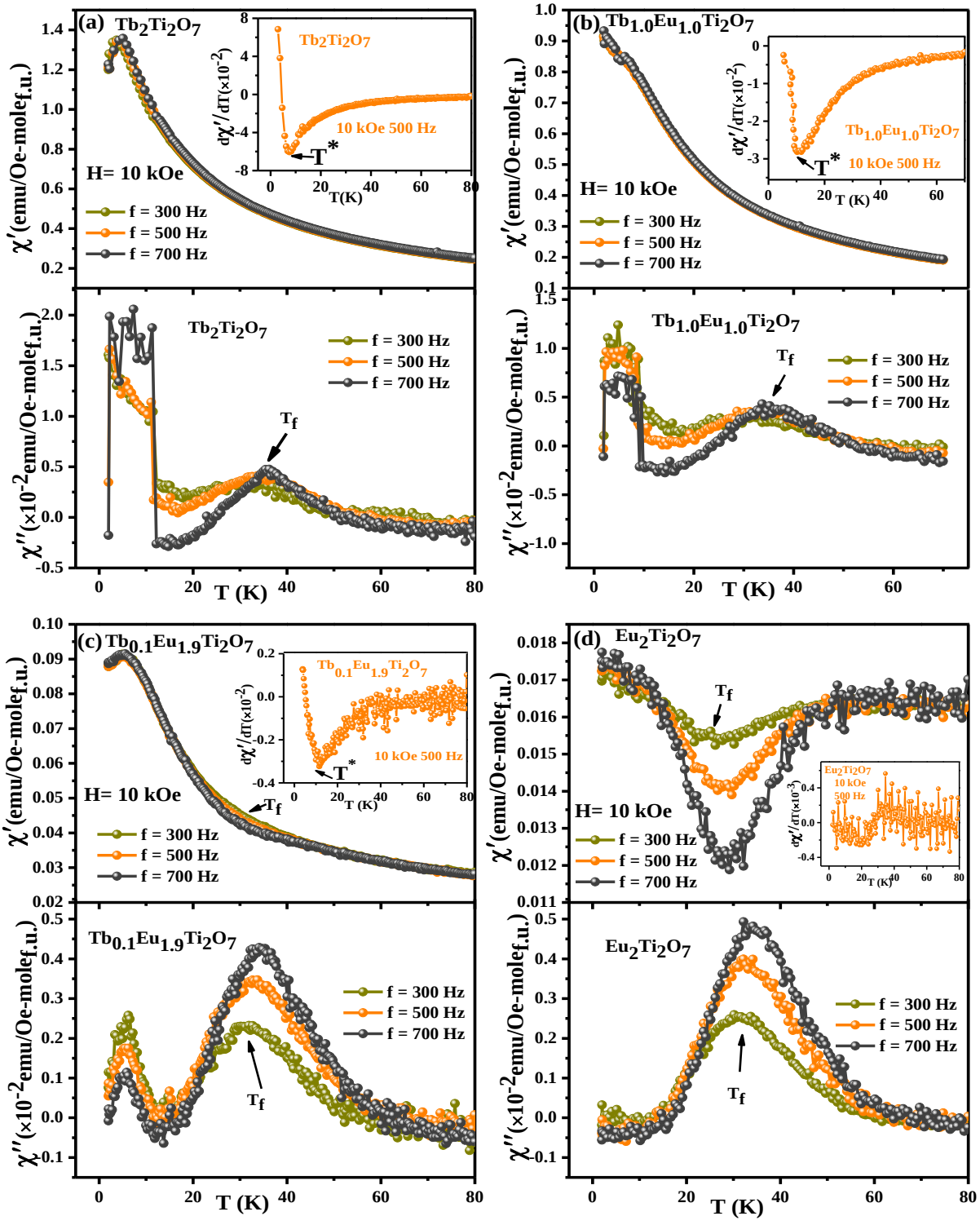

Figure 3.6: $\chi'(T)$ (upper panel) and $\chi''(T)$ (lower panel) of TETO compounds at applied field of 10 kOe. (a) x = 0.0, (b) x = 0.5, (c) x = 0.95, (d) x = 1.0. The inset in every upper panel: $d\chi'(T)/dT$ with T. Marked by arrow are: Single ion spin freezing peak (T_f) and Single moment saturation peak (T^*).

The same scenario is found for all other samples as the field induced transition appears at low temperature whereas the spin freezing transition is found at higher temperature as shown in Figure 3.6b and Figure 3.6c respectively. The irregular nature of field induced peak is common for x = 0.25 and x = 0. 50 samples except its position which shifts towards higher temperature (data for x = 0.25 sample is not shown here). This could be explained similarly to what is observed in TTO. For x = 0.90 and x = 0.95 samples, the spin freezing was observed even in the $\chi'(T)$ curves which possibly indicate towards relatively slower spin relaxation associated to the Eu^{3+} spins. The behaviour of low temperature peak in $\chi''(T)$ curve for x = 0.90 and x = 0.95 is similar to that for x = 0.00, x = 0.25 and x = 0.50 samples. However, in the x = 0.90 and x = 0.95 samples, this low temperature magnetic field induced peak is quite marked even in the same frequency range (<1 kHz) (data for x = 0.90 sample is not shown here). The unusual behaviour can be explained on the basis of stronger interaction between Tb-Eu ions than between Tb-Tb ions. Another explanation of this slow spin relaxation process for low temperature peak could be the presence of both dipolar and exchange interactions between Eu and Tb spins along with crystal field effect at low temperature as evidenced from DC magnetic analysis for particular (x= 0.90, 0.95) samples.

The low temperature field induced transition peak systematically shifts towards higher temperature with increasing Eu concentration. As the positions of this peak for all the samples are not so precise particularly in $\chi''(T)$. We have accomplished our whole analysis from $\chi'(T)$ measurement of all TETO samples. To verify and find the field induced transition temperature, we have taken the differentiation of real part of susceptibility with respect to temperature i.e, $d\chi'(T)/dT$ as shown in each inset of upper panel of Figure 3.6(a-d) at 500 Hz frequency. The minimum value or kink point has been taken as T^* temperature in all these

$d\chi'(T)/dT$ vs. T graphs. From this analysis, we have extracted the value of magnetic field induced transition temperature T^* (shown in the insets of Figure 3.6) for all samples and the variation of T^* with x has been presented in Figure 3.7b. From this graph, it can be concluded that magnetic field induced transition temperature increases with increase of Eu^{3+} concentration confirming that T^* systematically shifts towards higher temperature with Eu content. The shifting of T^* with Eu^{3+} doping is possibly due to a systematic change in the variation in the crystal field levels of Tb ions as the crystal field depends on the different structural parameters like - lattice constants and positional parameters of R^{3+} ions [43]. As reported earlier, ETO does not show any low temperature field induced transition [Figure 3.6d] [67].

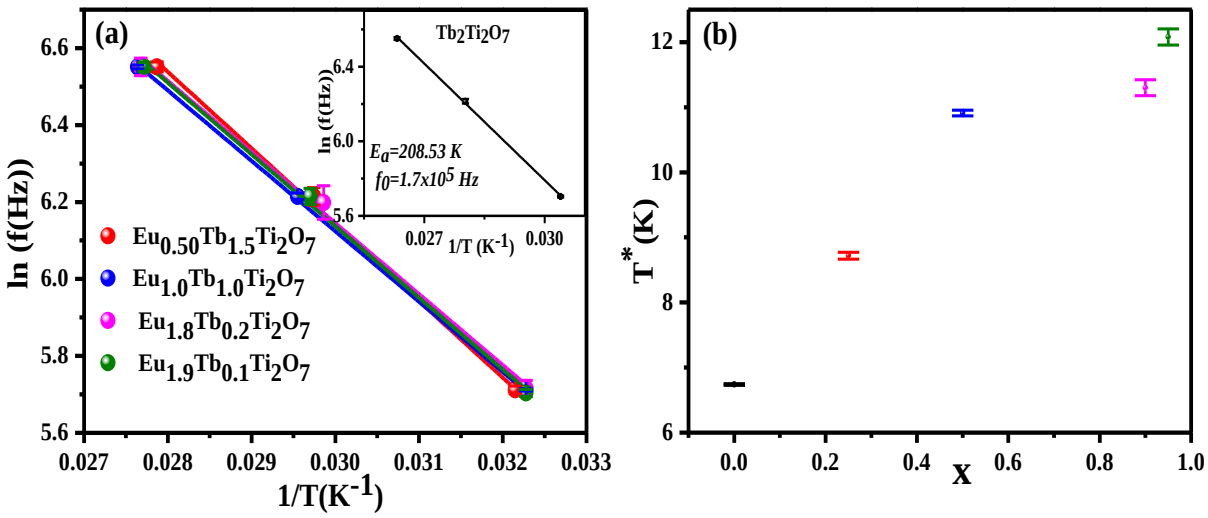

Figure 3.7(a): The Arrhenius Fit of (T_f) peak for compounds $(Tb_{1-x}Eu_x)_2Ti_2O_7$ (x = 0.25, 0.50, 0.90, 0.95). Inset: Arrhenius Fit of $Tb_2Ti_2O_7$. **(b):** Variation of field induced transition temperature T^* with Eu content (x) for TETO samples.

The T^* of TETO samples is independent of the frequency suggesting that it is not related to thermal relaxation process of spins. Not being thermally activated, it does not follow an

Arrhenius law. The nature of this peak for TETO samples is similar to that of pure TTO. Therefore, this new field induced transition could be associated with single moment saturation [45]. Similar field induced transition is also found for hybrid $Dy_xTb_{2-x}Ti_2O_7$ pyrochlore system where two distinct peaks, one at 16 K (single ion freezing) and another at 12 K (field induced) are found in AC susceptibility [194]. The peak at T_f = 33 K which is associated with weak spin freezing is also present in the $\chi''(T)$. The surprising point in the freezing peaks (T_f) is its position which remained almost unaltered i.e. positioned below 34 K for all TETO samples. There is no change in its position even in presence of magnetic field of 10 kOe except a little suppression has been observed in the spin freezing which again confirms single ion spin freezing nature. Further study may help to get the exact origin of the observed higher temperature spin freezing in TTO pyrochlore and to know the unrevealed concepts of spin relaxation mechanism.

3.4 Conclusion:

We have systematically studied the structural, Raman Effect and magnetic properties of $(Tb_{1-x}Eu_x)_2Ti_2O_7$ (with x= 0, 0.25, 0.50, 0.90, 0.95, 1.0) pyrochlore system. The formation of all the compositions and the systematic substitution of Tb^{3+} by Eu^{3+} ions have been analyzed from structural and Raman studies. The DC magnetization study has shown an enhancement of antiferromagnetic interaction and a decrease in total magnetic moment with Eu doping. AC magnetic susceptibility study of $Tb_2Ti_2O_7$ has shown a single ion weak spin freezing at T_f = 33 K at zero magnetic field. For the other samples, a similar spin freezing has also been found. On applying a field of 10 kOe, all the compounds have shown a new field induced transition T^* which shifts towards higher temperature on increasing the concentration of Eu ions. This field induced transition corresponds to single moment saturation.